Hindawi
Advances in Materials Science and Engineering
Volume 2019, Article ID 6578350, 7 pages
https://doi.org/10.1155/2019/6578350

Research Article

The Effect of Yttrium Addition on the Microstructures and Electrical Properties of CuMn Alloy Thin Films

Ho-Yun Lee,[1] Chi-Wei He,[2] and Ying-Chieh Lee[2]

[1]*Department of Material Science and Engineering, École Polytechnique Fédérale de Lausanne, Lausanne, Switzerland*
[2]*Department of Materials Engineering, National Pingtung University of Science & Technology, Pingtung 91201, Taiwan*

Correspondence should be addressed to Ying-Chieh Lee; yclee@mail.npust.edu.tw

Received 22 July 2019; Revised 11 October 2019; Accepted 28 October 2019; Published 20 November 2019

Academic Editor: Pavel Lejcek

In this study, we fabricated thin-film resistors using CuMn and yttrium targets by DC/RF magnetron cosputtering. CuMnY-resistive thin films were deposited onto glass and Al_2O_3 substrates. The electrical properties and microstructures of CuMn alloy films with different yttrium content were investigated. The CuMnY films were annealed at temperature ranging from 250°C to 350°C in N_2 atmosphere. The phase variation, microstructure, film thickness, and constitutional analysis of CuMnY films were characterized using X-ray diffraction, field emission scanning, and high-resolution transmission electron microscopy and related energy dispersive X-ray analyses (XRD, FESEM, and HRTEM/EDX). It was found that CuMnY alloy films separated into two parts after annealing. The first part is the MnO phase on the bottom side of the film. The second part is an amorphous structure on the upper side of the film. The MnO phase is a microcrystalline that exists in CuMn films, which is dependent on the Y content and annealing temperature. CuMn alloy films with 15.7% yttrium addition annealed at 300°C exhibited higher resistivity ~4000 $\mu\Omega$-cm with −41 ppm/°C of temperature coefficient of resistance (TCR).

1. Introduction

High-speed technological advancements have occurred rapidly in the electronics industry, such as in telecommunication, information, and aerospace. The precision measurement sector of industry requires continuous electronic components development to achieve higher precision, reliability, and integration [1]. There are some advantages for thin-film resistors such as high accuracy and low noise, low temperature coefficient of resistance (TCR), good heat resistance, and stability, which make them widely used in precision electronic instruments. The resistive film in thin-film resistors is deposited onto a ceramic or glass matrix using a sputtering process [2–4].

Copper-manganese alloy films are used in mobile electronic devices because of their high thermal stability and low resistance. Copper has low electrical resistivity while manganese has thermal stability in this CuMn alloy system [5]. Based on the equilibrium phase diagram, there are no intermetallic phases in the CuMn system. Copper can serve as a substitute species for Mn in the FCC lattice [6]. A characteristic feature of Mn in Cu is its larger activity coefficient compared with other elements that have limited solubility, such as Al and Mg [7]. However, Mn does not tend to precipitate or segregate within the Cu film but can easily diffuse out to the surface and interface under oxidative conditions [8].

The specific resistivity of CuMn films was measured over the whole composition range [9]. The resistivity of pure manganese and copper films was 174 $\mu\Omega$-cm and 1.7 $\mu\Omega$-cm, respectively. The $Cu_{0.2}Mn_{0.8}$ alloy films have a maximum resistivity of 205 $\mu\Omega$-cm with a temperature coefficient of resistance (TCR) of −308 ppm/°C. Focusing on the electrical properties of $Cu_{0.5}Mn_{0.5}$ alloy films, the resistivity was about 137 $\mu\Omega$-cm with a TCR of −377 ppm/°C. There is a higher TCR value in the CuMn alloy films. However, the low TCR property is one of the most important qualities of resistors for electronic circuits [10].

To improve CuMn-resistive film electrical properties, foreign elements are added into the CuMn alloy films during

cosputtering. Lee et al. studied the electrical properties of Cu-Mn films with different amounts of Dy addition. Cu-Mn films with 40 at.% Dy addition that were annealed at 300°C exhibited a resistivity of ~2100 $\mu\Omega$-cm with the smallest temperature coefficient of resistance (−85 ppm/°C) [11]. Yttrium was chosen as the dopant in the current work because of its high melting point (1526°C) and thermal stability, which may be advantageous for resistive thin film thermal stability. The phase, microstructure, and electrical property of CuMn thin films with different yttrium content are investigated in this study.

2. Experimental Procedure

2.1. CuMnY Thin-Film Preparation. CuMnY thin films with a thickness of 80 nm were prepared onto substrates using a direct current (DC) radio frequency (RF) magnetron cosputtering system. A $Cu_{0.5}Mn_{0.5}$ alloy target with 99.95% purity was set at the DC position with a yttrium target with 99.9% purity set at the RF position. The target diameter was 76.2 mm. The DC power was fixed at 50 W with the RF power changed in range from 60 W to 100 W. A background pressure of 4×10^{-7} torr in the sputtering chamber was maintained using a cryo-pump. Argon gas was executed with a purity of 99.999% at a flow rate of 60 sccm using mass flow controllers with 3×10^{-3} torr working pressure maintained. Glass substrates $20 \times 10\,mm^2$, silicon wafers $10 \times 10\,mm^2$, and Al_2O_3 substrates were used for the sheet-resistance measurement, film thickness analysis, and TCR measurements, respectively. Alumina substrates with cell sizes of 1.6×0.8 mm printed Ag electrodes were used in this study. The as-deposited films were annealed at 250, 300, and 350°C for 2 hours at a heating rate of 5°C/min in N_2 atmosphere. N_2 gas with a purity of 99.99% was used in this study.

2.2. Analysis. The sheet resistance R_s is usually used to characterize material resistivity using thin-film deposition. The four-point probe technique is the measurement method. The film thickness is measured after cosputtering using field-emission scanning electron microscopy (FE-SEM, Hitachi S-4700 Japan) on a film cross section. The thin-film TCR values were measured on long thin strips cleaved from the substrate. Electrical contacts at the two ends of the resistive strips were obtained by selectively coating the ends with sputtered silver. The DC resistance of the strips was measured using a digital multimeter (HP 34401A) at different temperatures (25°C and 125°C). The thin-film TCR was measured using the following equation [11]:

$$\mathrm{TCR} = \left[\frac{\Delta R}{\Delta T} \times \frac{1}{R}\right] \times 10^6 \mathrm{ppm/K}. \quad (1)$$

X-ray diffraction (XRD, Bruker D8A Germany) was used to determine the crystalline phases. An electron probe microanalyzer (EPMA, JEOL JXA-8900R Electron Probe X-ray Microanalyzer) was used to analyze the film compositions. Microstructural, selected-area diffraction (SAD) patterns, and EDX (energy dispersive X-ray spectroscopy) analysis of the specimens were executed using a field-emission transmission electron microscopy (FE-TEM, FEIE.O. Tecnai F20) equipped with an energy dispersive spectrometer at an accelerating voltage of 200 kV.

3. Results and Discussion

CuMnY films were prepared using a DC and RF magnetron cosputtering system. The composition of as-deposited thin films at different RF powers was analysed using the electron probe microanalyser (EPMA). The results are listed in Table 1. The results showed that by increasing the RF sputtering power, the Y to CuMn content ratio tends to increase while the CuMn content decreased and the Y content increased. As the RF sputtering power increases from 60 W to 100 W, the Y content increases from 8.7 at.% to 19.6 at.% in the CuMn thin films. The yttrium growth rate increased with increasing RF sputtering power. At higher powers, the bombarding ions will have higher kinetic energy because of momentum transfer, and the target atoms will be sputtered out. Significantly more species will be ejected from the target, resulting in a higher deposition rate.

X-ray diffraction data from the as-deposited and annealed samples with different yttrium content are presented in Figure 1. The increase in scattered intensity at $2\theta = \sim 41^\circ$ is related to the MnO (200) for CuMn films annealed at 250°C in N_2 atmosphere. However, all of the CuMnY films annealed at 250°C in N_2 atmosphere have an amorphous structure as shown in Figure 1(a). When the annealing temperature was increased up to 300°C, Cu and MnO phases were observed in the pure CuMn alloy films. However, there is a Cu crystallization phase with a (111) peak observed only in CuMn films with 19.6 at.% yttrium, as shown in Figure 1(b). The increase in MnO peak scattered intensity was observed at 350°C in pure CuMn alloy films. This means that CuMn alloy films critically oxidized. According to Bragg's law and selection rule, 2θ values of the first three diffraction peaks (111), (200), and (220) of MnO rock salt-structured using Cu k_α radiation are located at 35.1°, 40.3°, and 58.7°, respectively. Note that a Cu crystallization phase existed only in the CuMn films at 350°C when yttrium was added at ≥15.7%, as shown in Figure 1(c). This indicates that yttrium addition in CuMn films leads to film oxidation resistance.

Transmission electron microscopy (TEM) analysis was performed to determine the specimen crystallographic structure. Diffraction pattern analysis and corresponding images from the SAD patterns are commonly applied to identify the sample crystallinity and orientation. Figure 2 is a cross-sectional TEM micrograph of the pure CuMn sample after 350°C annealing in nitrogen atmosphere. The film thickness was found to be about 60 nm as shown in Figure 2(a). However, the sample was separated into two parts, a top layer and a bottom layer. In the bottom layer, SAD analysis shows MnO crystallites in Figure 2(b). The Cu_2O phase was detected in the top layer according to SAD analysis and high-resolution TEM micrograph, as shown in Figures 2(c) and 2(d). This phenomenon was explained by Lee et al. [12].

Table 1: CuMnY thin-film composition prepared at DC 50 W with different RF powers sputtered onto cooper sheet.

Power (W)	DC/RF	50/60	50/80	50/100
Element (at%)	Cu	61.3	54.7	52.6
	Mn	30	29.6	27.8
	Y	8.7	15.7	19.6

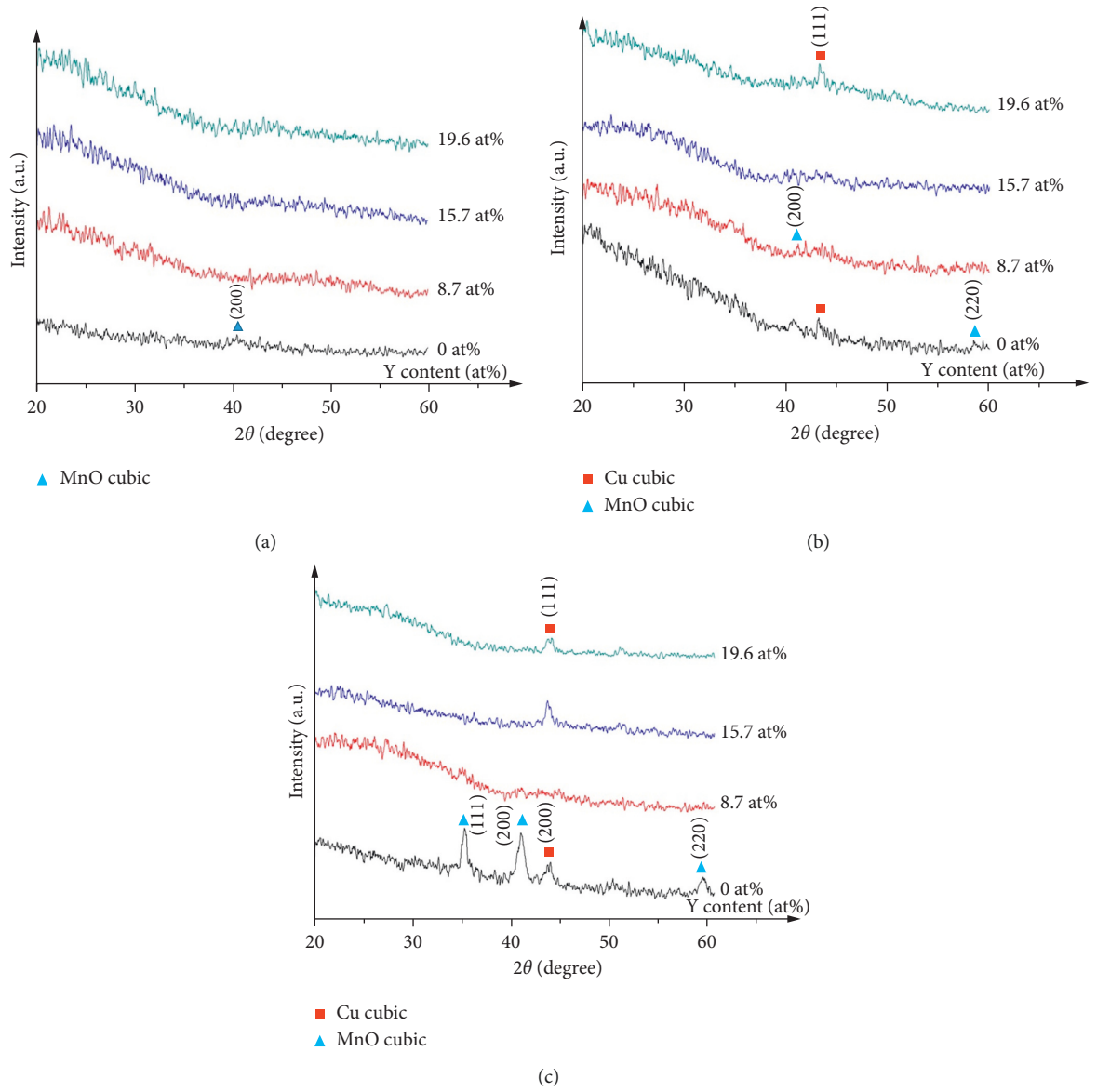

Figure 1: CuMnY thin-film X-ray diffraction patterns with various amounts of yttrium addition annealed at (a) 250°C, (b) 300°C, and (c) 350°C.

Figure 3 shows the CuMn alloy films with 8.7 at.% Y addition annealed at 300°C for a cross-section TEM micrograph and SAD analysis. It is clear that microcrystalline phases 5–10 nm in diameter are present on the bottom layer as shown in Figure 3(b). The oxide particles, identified as MnO by SAD pattern analysis, are shown in Figure 3(c). This layer was oxidized by oxygen that came from the substrate. On the film top side, an amorphous structure existed in the CuMnY film from high-resolution transmission electron microscopy analysis. This result is consistent with the XRD analysis (Figure 1(b)). Mn is a transition metal, having variable valence, and hence, Mn can be found in different oxidation states (Mn^{2+}, Mn^{3+}, and Mn^{4+}). Different crystalline phases such as MnO, MnO_2, Mn_2O_3, and Mn_3O_4 exist [13]. Figure 4 shows CuMn alloy films with 19.6 at.% Y addition annealed at 300°C for a cross-section TEM micrograph and SAD analysis. With yttrium addition up to 19.6 at.%, some microcrystalline phases with ~5 nm in diameter on the bottom side still are observed as shown in Figure 4(b). SAD pattern analysis showed that the

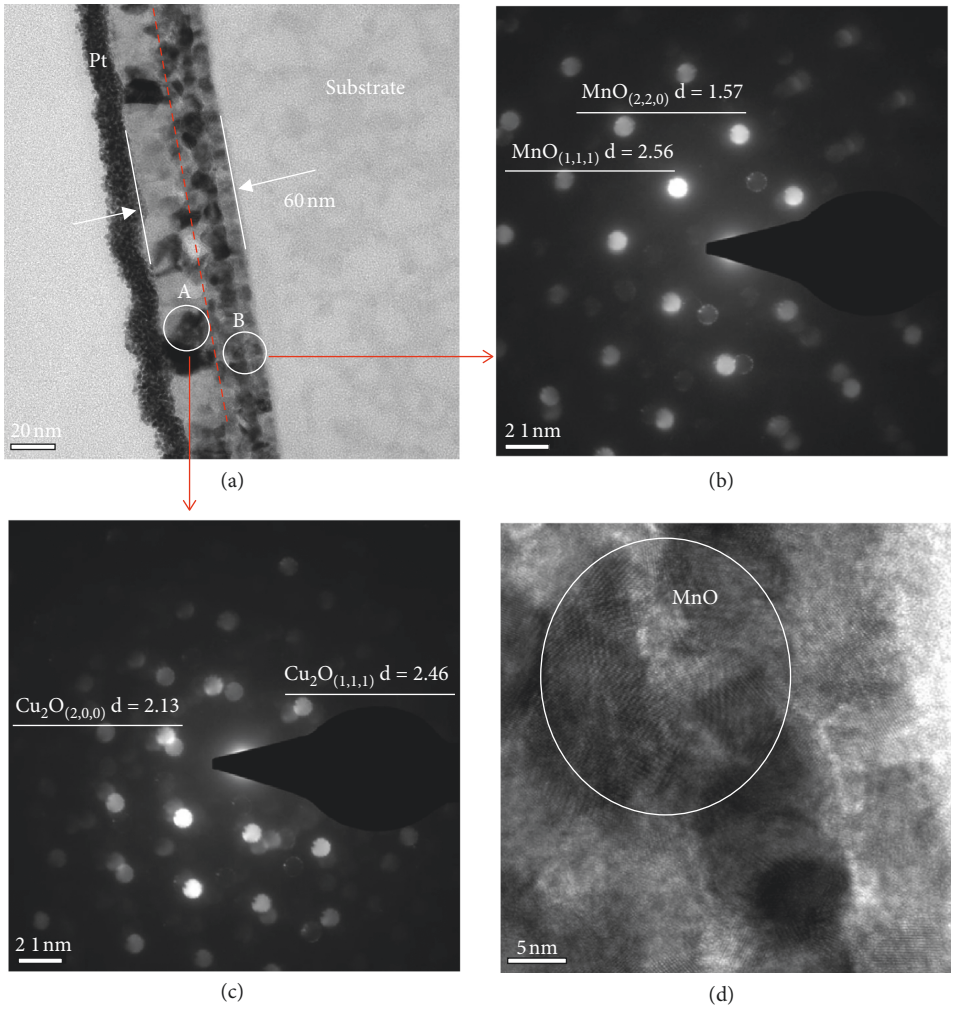

Figure 2: CuMn film TEM micrographs annealed at 350°C: (a) cross-section bright field, (b) selected-area electron diffraction at position A, (c) selected-area electron diffraction at position B, and (d) HRTEM micrographs at position B.

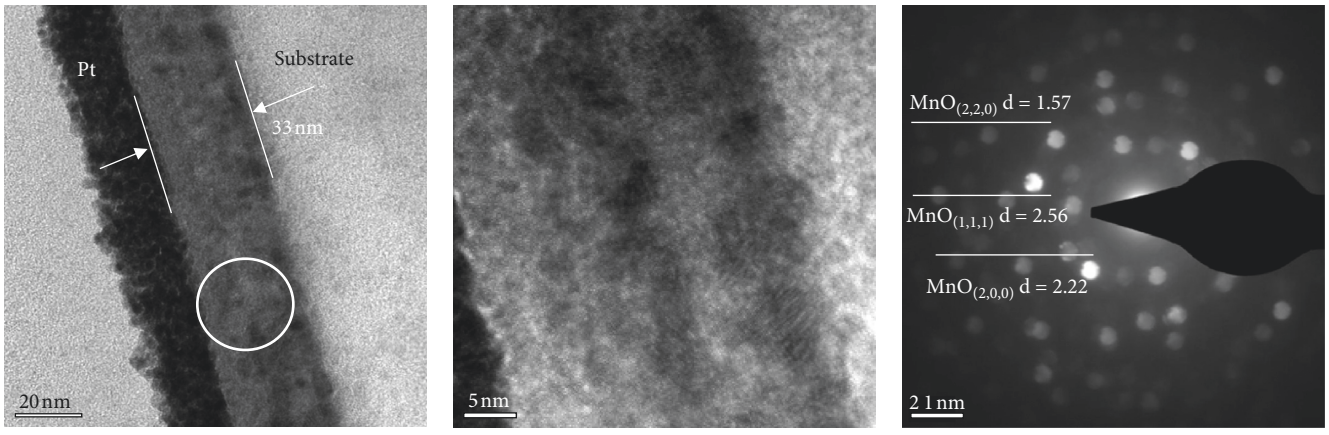

Figure 3: CuMn film TEM micrographs with 8.7 at.% Y addition annealed at 300°C: (a) cross-section bright field, (b) selected-area electron diffraction, (c) SAD analysis, and (d) HRTEM micrographs.

microcrystalline phases belonged MnO phase as shown in Figure 4(c). However, MnO crystallinity obviously decreased in CuMn films with 19.6 at.% Y addition compared with 8.7 at.% Y addition. This means that the oxidation level in CuMn films is dependent on the Y addition. This result indicates that more Y added into CuMn alloy films can reduce MnO

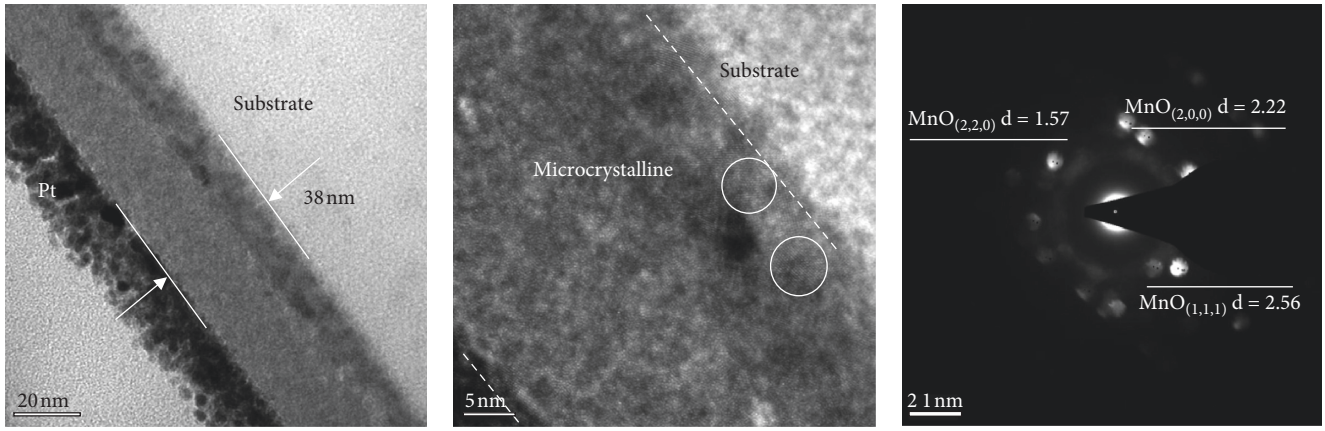

(a) (b) (c)

Figure 4: CuMn film TEM micrographs with 19.6 at.% Y addition annealed at 300°C: (a) cross-section bright field, (b) selected-area electron diffraction, (c) SAD analysis, and (d) HRTEM micrographs.

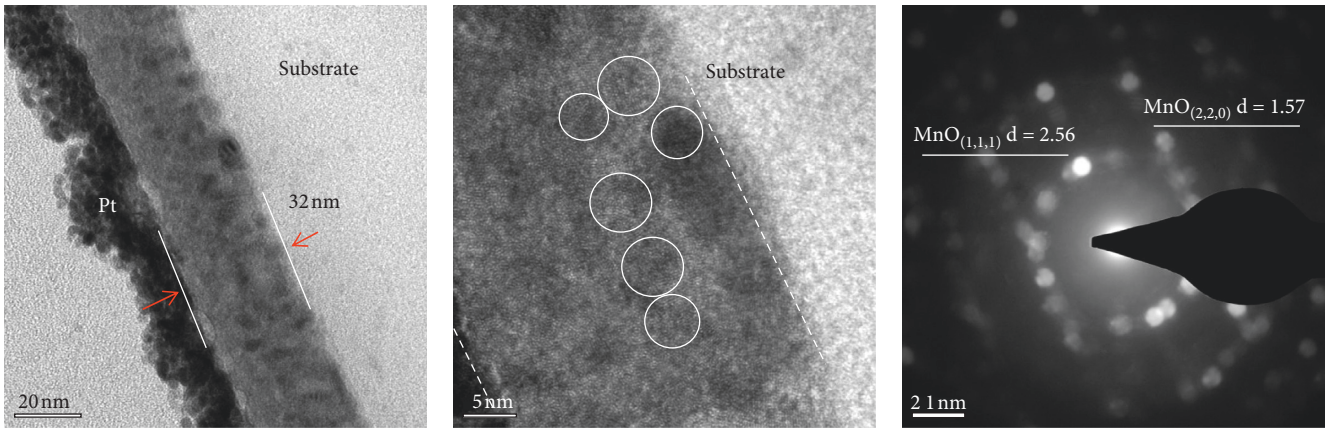

(a) (b) (c)

Figure 5: CuMn film TEM micrographs with 19.6 at.% Y addition annealed at 350°C: (a) cross-section bright field, (b) selected-area electron diffraction, (c) SAD analysis, and (d) HRTEM micrographs.

formation. Figure 5 shows a cross-sectional TEM bright field micrograph and SAD analysis of the CuMn alloy films with 19.6 at.% Y addition annealed at 350°C. With increasing annealing temperature up to 350°C, there is more microcrystallinity on the bottom side observed as shown in Figure 5(b), and the film still has an amorphous structure on the upper side. The oxidation compounds were still MnO phases according to the SAD pattern analysis as shown in Figure 5(c). Unlike CuMn alloy films (all the films were crystallized or oxidized), we found that an amorphous structure still existed in CuMnY annealed films. This may be due to the multiple element alloy effect, which can be explained by the kinetics theory because of slow atomic diffusion [14, 15]. Yttrium addition in CuMn films leads to the formation of an amorphous structure and reduced oxidation after annealing at 350°C.

Figure 6 shows the effects of yttrium addition on the resistivity of CuMn alloy films at different annealing temperatures. Yttrium addition can significantly enhance CuMn film resistivity. This is due to a gradual decrease in CuMnY alloy film copper with increasing yttrium (Table 1). Wang et al. reported that yttrium can cause grain refinement in the Y-Cu system during mechanical alloying [16]. However, it is well known that a decrease in the grain size can enhance the grain boundary and therefore increase the electrical resistivity [17]. The resistivity of yttrium and copper is 56 $\mu\Omega$-cm and 1.7 $\mu\Omega$-cm, respectively. Yttrium addition could enhance CuMn film resistivity. On the other hand, an alloy film amorphous structure can be obtained by yttrium addition. This phenomenon also enhances CuMnY film resistivity [16]. However, with the increase in annealing temperature, CuMnY film resistivity increased. The alloy film resistivity increases because the film grain boundaries, crystal defects, and generated oxides increased when the annealing temperatures were increased [17]. Figure 7 shows the yttrium addition and annealing temperature effects on the CuMn film temperature coefficient of resistivity. Misják et al. reported that TCR shows a negative value after Mn added at amounts higher than 20% to Cu because of the presence of disordered structures that lead to lower

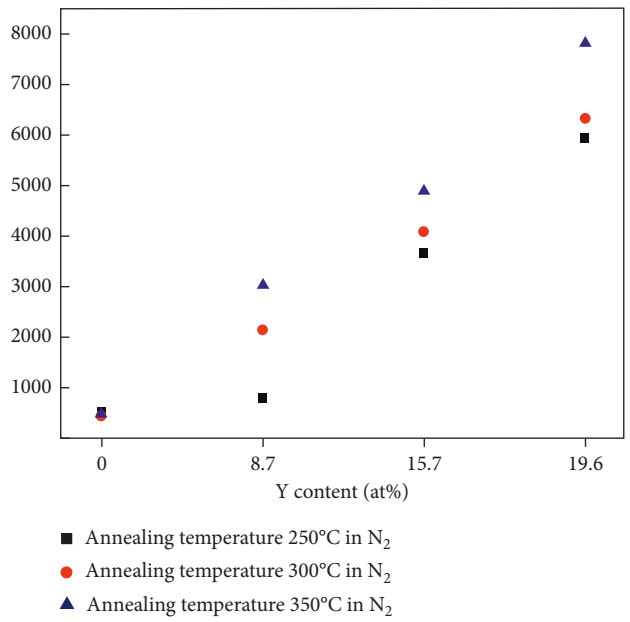

Figure 6: CuMn film room temperature resistivity with various yttrium contents annealed at different temperatures.

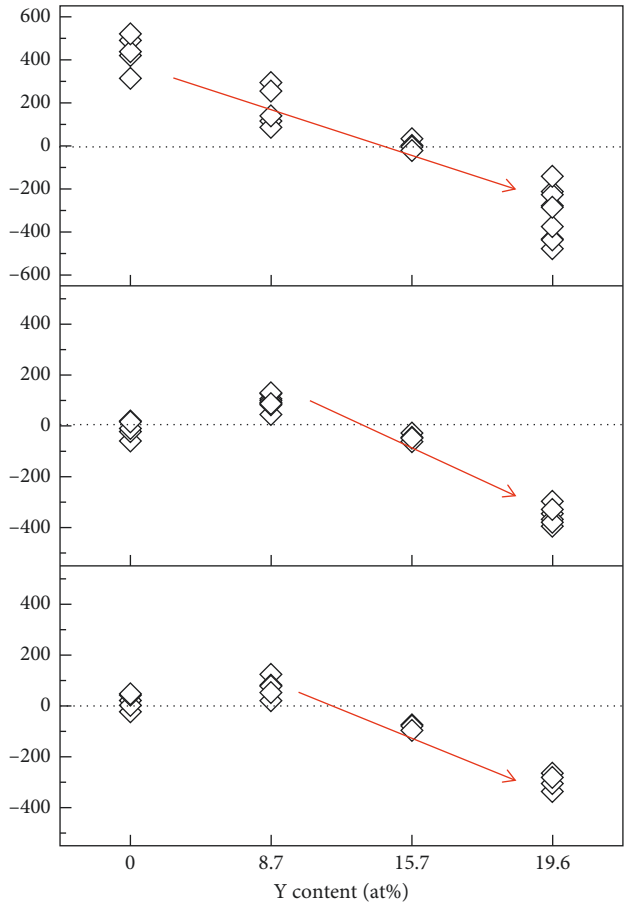

Figure 7: CuMn film TCR temperature dependence with various yttrium contents annealed at different temperatures.

conductivity [9]. It was found that the TCR changes significantly from a positive value to negative value with increasing yttrium content at annealing temperatures from 250°C to 350°C. This phenomenon indicates that the TCR value is influenced by the yttrium content in CuMn films.

4. Conclusion

The annealing temperature and Y content effects on CuMnY thin-film electrical properties were investigated in this study. Two layers exist in CuMnY films at ≥300°C annealing in N_2 atmosphere. The first layer is an amorphous layer on the upper side. The second layer is a MnO phase on the bottom side. The MnO microcrystalline phase exists in CuMn films dependent on the amount of Y addition and annealing temperature. Unlike CuMn alloy films, an amorphous structure exists in CuMnY annealed films. This may be due to the multiple element alloy effect. Yttrium addition in CuMn films leads to the formation of an amorphous structure and reduces oxidation after annealing. CuMn films with 15.7 at.% yttrium addition annealed at 300°C exhibited a resistivity of ~4000 $\mu\Omega$-cm with the smallest temperature coefficient of resistance (−41 ppm/°C).

Data Availability

The data used to support the findings of this study are available from the corresponding author upon request.

Conflicts of Interest

The authors declare that they have no conflicts of interest.

Acknowledgments

The authors would like to acknowledge financial support of this research from the Ministry of Science and Technology of Taiwan under contract no. 106-2221-E-020-009.

References

[1] B.-J. Lee and D.-C. Lee, "Electrical properties of sputtered Ni-Cr-Al-Cu thin film resistors with Ni and Cr contents," *Journal of the Korean Physical Society*, vol. 40, p. 339, 2002.

[2] T. Miyata, S. Tsukada, and T. Minami, "Preparation of anatase TiO_2 thin films by vacuum arc plasma evaporation," *Thin Solid Films*, vol. 496, no. 1, pp. 136–140, 2006.

[3] G. Katumba and L. Olumekor, "Effects of thickness and composition on the resistivity of Cu-MgF2 cermet thin film resistors," *Journal of Materials Science*, vol. 35, no. 10, pp. 2557–2559, 2000.

[4] Y. Noriaki, O. Yukiko, H. Tohru, and Y. Shu, "Fabrication of CeO_2 thin film on quartz glass and MgO(100) by electron beam evaporation," *Solid State Ionics*, vol. 172, p. 293, 2004.

[5] E. M. Kim, S. C. Kim, and S. Lee, "Electrical properties of Cu/Mn alloy resistor with low resistance and thermal stability," *Journal of the Korean Institute of Electrical and Electronic Material Engineers*, vol. 29, no. 6, pp. 365–369, 2016.

[6] W. B. Pearson, *A handbook of lattice Parameters and structures in metals and alloys*, Vol. 1, Pergamon Press, London, UK, 1958.

[7] J. Iijima, Y. Fujii, K. Neishi, and J. Koike, "Resistivity reduction by external oxidation of Cu-Mn alloy films for semiconductor interconnect application," *Journal of Vacuum Science & Technology B: Microelectronics and Nanometer Structures*, vol. 27, no. 4, p. 1963, 2009.

[8] C.-Y. Wu, C.-T. Wu, W.-H. Lee, S.-C. Chang, and Y.-L. Wang, "A study on annealing mechanisms with different manganese contents in CuMn alloy," *Journal of Alloys and Compounds*, vol. 542, pp. 118–123, 2012.

[9] F. Misják, K. H. Nagy, P. Lobotka, and G. Radnoczi, "Electron scattering mechanisms in Cu-Mn films for interconnect applications," *Journal of Applied Physics*, vol. 116, no. 8, p. 083507, 2014.

[10] P. L. Kirby, "Applications of resistive thin films in electronics," *Thin Solid Films*, vol. 50, pp. 211–221, 1978.

[11] H.-Y. Lee, C.-W. He, Y.-C. Lee, and D.-C. Wu, "A study on the characteristics of Cu–Mn–Dy alloy resistive thin films," *Coatings*, vol. 118, p. 1, 2019.

[12] N.-C. Chuang, J.-T. Lin, and H.-R. Chen, "TCR control of Ni-Cr resistive film deposited by DC magnetron sputtering," *Vacuum*, vol. 119, pp. 200–203, 2015.

[13] H. Jamil, M. Khaleeq-ur-Rahman, I. M. Dildar, and S. Shaukat, "Structural and optical properties of manganese oxide thin films deposited by pulsed laser deposition at different substrate temperatures," *Laser Physics*, vol. 27, no. 9, p. 096101, 2017.

[14] Y. Zhang, Y. J. Zhou, J. P. Lin, G. L. Chen, and P. K. Liaw, "Solid-solution phase formation rules for multi-component alloys," *Advanced Engineering Materials*, vol. 10, no. 6, pp. 534–538, 2008.

[15] M.-H. Tsai, C.-W. Wang, C.-W. Tsai et al., "Thermal stability and performance of NbSiTaTiZr high-entropy alloy barrier for copper metallization," *Journal of the Electrochemical Society*, vol. 158, p. H1161, 2011.

[16] B. Wang, Y. Zhang, B. Tian et al., "Effects of Ce addition on the Cu-Mg-Fe alloy hot deformation behavior," *Vacuum*, vol. 155, p. 594, 2018.

[17] H. Zeng, Y. Wu, J. Zhang, C. Kuang, M. Yue, and S. Zhou, "Grain size-dependent electrical resistivity of bulk nanocrystalline Gd metals," *Progress in Natural Science: Materials International*, vol. 23, no. 1, pp. 18–22, 2013.